Nonequilibrium air flow predictions with a high-fidelity direct simulation Monte Carlo approach

Sergey F. Gimelshein[1,*] and Ingrid J. Wysong[2]
[1]*ERC Inc., Edwards AFB, California 93524, USA*
[2]*Aerospace Systems Directorate, AFRL, Edwards AFB, California 93524, USA*

(Received 31 August 2018; published 29 March 2019)

A conventional and a high fidelity direct simulation Monte Carlo approach of internal energy transfer and chemical reactions are considered in application to a number of cases where validation data are available. Normal shock wave, hypersonic flow over a wedge, a sphere, and a double cone are considered, and measured and computed flow and surface properties are compared. The primary objective is to examine the impact of the model of each particular physical process which contributes to flow thermal and chemical nonequilibrium. For the considered conditions, with free stream gases of oxygen, nitrogen, and air, flow velocities ranging from 3 to 6 km/s, and Knudsen numbers on the order of 0.001, the change in the internal energy transfer and chemical reaction models was found to have a relatively small effect on the surface properties. The only notable exception is nitrogen gas-phase recombination, which drastically increases the heat flux to the wall.

DOI: 10.1103/PhysRevFluids.4.033405

I. INTRODUCTION

Recent advancements in hypersonic research provide solid ground for studying one of the key components and determining features of hypersonic flow, namely, thermochemical nonequilibrium. Flow nonequilibrium, exhibited in thermal effects related to the excitation of internal degrees of freedom of gas molecules, and chemical effects of unbalanced reactions and electronic transitions, plays an important, and often determining, role in high Mach, moderate Reynolds number flows that typically occur in hypersonic flight. Physical, chemical, and gasdynamic issues that stem from the above real-gas effects are adding to the complexity of nonequilibrium flow, and traditionally make it not easily amenable to computational investigation.

There are several factors contributing towards the progress in high-temperature nonequilibrium flow research. First, the ongoing experimental work in several established shock tube facilities [1–5] complements and expands the research conducted at the end of the 20th century [6–8]. While the earlier measurements still carry significant value and are important for flow analysis and model validation, the new studies take advantage of more recent accurate techniques and instruments, promise to offer longer test times, and in many cases are capable of providing better characterization of flow conditions, especially those in the free stream. The latter is especially true for newly built and under-development facilities, such as LENS-XX [9], X3 [10], and T6 [11], which noticeably expand the parameter space for hypervelocity research. They provide an opportunity for examination of relatively rarefied, and thus highly nonequilibrium, flows with free stream densities on the order of 1 g/m^3 and lower, at flow velocities from as low as 3 km/s to as high as 18 km/s.

The second factor important for gaining insight into key peculiarities and features of nonequilibrium flows is computational chemistry. In the last few years, there has been significant effort aimed at better understanding of thermal processes of air species, and much recent work has examined

*particlemattersinc@gmail.com

improved potential energy surfaces and internal energy excitation and collisional dissociation at the detailed state-to-state trajectory calculation and direct molecular dynamics level. Examples here are Refs. [12–14] for N_2-N_2 collisions, Refs. [15,16] for N_2-N, Refs. [17,18] for O_2-O, and most recently, Ref. [19] for O_2-O_2. Studies of Zeldovich exchange reactions have also been conducted, with quasiclassical trajectory calculations (QCT) for nitric-oxide producing reactions [20] complementing previous results [21,22]. Although there are several reactive collision types, such as those that include nitric oxide, which still lack detailed QCT information, the currently available *ab initio* database of internal energy transfer and chemical reaction cross sections and rates arguably covers most of the key inelastic collision processes that influence gas and surface properties of high-temperature nonionized air flows.

Newly available experimental data and high-quality detailed microscopic-level information on inelastic collision processes in high-temperature air have stimulated the development of microscopic, kinetic models of those processes [23–26] that promise to exceed the fidelity of the earlier models, and thus have a potential to improve accuracy of nonequilibrium flow prediction. Practically all these models are suitable or developed specifically for the direct simulation Monte Carlo (DSMC) method. That does not come as a surprise since the DSMC method is conventionally looked at as the most powerful approach for modeling flows with significant degree of rarefaction and thus nonequilibrium. Clearly, the DSMC method's unsurpassed convenience of adding new collisional models has also played a role here. With the number of DSMC-fitted models for nonequilibrium flows proliferating, the question is now not only what model to choose, but rather how much detail is enough or, in other words, what are the key physics that must be captured to reasonably model the important characteristics of these flows?

It seems that the only way to answer that question is to perform a model-to-model comparison paired with a model-versus-data validation, so that the former allows one to assess what effects are important, while the latter provides a way to discriminate fidelity of important physics between models. The present work is a step in that direction, and its main objective is to examine the importance of the model for a number of processes peculiar to high-temperature air flows. These processes are vibration-vibration and vibration-translation energy transfer and chemical reactions of dissociation and recombination. The cases examined range from homogeneous bath relaxation to normal shock wave to axially symmetric flows over simple but indicative geometries. Available detailed QCT results and measurement data are used in comparisons, as they offer an opportunity to highlight situations where further model improvement may be necessary.

A conventional and a high-fidelity DSMC approach are used in this work, which provides an opportunity to evaluate the impact of the real gas effect model in nonequilibrium reacting flows. Note that it is important to differentiate between the impact of the nonequilibrium model and the impact of the equilibrium rate. A model represents a specific method or algorithm that describes a particular aspect of the inelastic collision process, such as a chemical transformation or transfer of energy between translational and internal molecular modes. It closely relates to cross sections, either total or differential, and thus is expected to be important in nonequilibrium situations. An equilibrium rate, either chemical or inelastic, determines the speed at which the corresponding process proceeds at equilibrium. Since the objective of this work is the analysis of the impact of the model, both conventional and the high-fidelity DSMC approaches used here are based on similar (and where possible identical) equilibrium rates. The rates, in turn, use state-of-the art experimental and QCT results, and thus the conventional DSMC here uses updated, compared to the older DSMC [27], rates.

II. NUMERICAL MODELS

A. Direct simulation Monte Carlo method

The numerical approach of choice in this work is the direct simulation Monte Carlo method [27], which allows for a straightforward implementation and testing of models at the kinetic level of

TABLE I. VHS model parameters for air species. First number in each cell is the collision diameter in Å at a reference temperature of 273 K, and the second is the temperature exponent.

	N	O	N_2	O_2	NO
N	3.000/0.75	$3.229 \times 10^{-10}/0.75$	$3.734 \times 10^{-10}/0.75$	$3.535 \times 10^{-10}/0.76$	$3.600 \times 10^{-10}/0.77$
O		$3.458 \times 10^{-10}/0.76$	$3.360 \times 10^{-10}/0.75$	$3.442 \times 10^{-10}/0.75$	$3.829 \times 10^{-10}/0.77$
N_2			$4.467 \times 10^{-10}/0.75$	$4.269 \times 10^{-10}/0.76$	$4.334 \times 10^{-10}/0.765$
O_2				$3.985 \times 10^{-10}/0.71$	$4.135 \times 10^{-10}/0.78$
NO					$4.200 \times 10^{-10}/0.79$

energy-dependent cross sections and energy-mode disposal over products of inelastic and reactive collisions. A parallel DSMC-based tool SMILE [28] is used in all computations. Since the primary target of the work is high-temperature processes, simplified models are used for elastic and rotationally inelastic collisions, as well as gas surface collisions. The variable hard sphere (VHS) model [29] is applied with interaction parameters listed in Table I, calculated from the viscosity-temperature data of Ref. [30]. Note that the parameter array is symmetric, and thus only its upper diagonal part is shown. Discretized rotational and vibrational energies are used, with 198 rotational and 59 vibrational levels for N_2 and 169 rotational and 46 vibrational levels for O_2. The rotational energy levels were assigned using the rigid rotator model, and the Morse anharmonic oscillator is used to define the vibrational levels. The discrete-energy Larsen-Borgnakke (LB) model [31,32] is applied for the rotation-translation (R-T) energy transfer, with temperature-dependent rotational relaxation numbers described in Refs. [33,34]. An implementation of LB prohibiting double relaxation [35,36] is used here. All gas-surface collisions are assumed to be diffuse with the full energy and momentum accommodation. Note that the above models capture realistic viscosity-temperature dependence and rotation-translation relaxation rates, and the impact of the model uncertainty on relatively high density reactive flows considered here is therefore negligible.

The number of simulated particles, the collision cell size in the adaptive grid, and the time steps used in the DSMC computations varied depending on the free stream conditions and flow dimensionality. Typically, on the order of 10 million molecules were taken in spatially homogeneous and one-dimensional flows, and about 500 million molecules in two-dimensional and axially symmetric flows. The number of collision cells was approximately five times smaller than the number of molecules, while the time step was selected so that particles do not cross more than one-half of one collision cell per one time step. In all cases considered, sensitivity studies were conducted to the parameters of the approach in order to exclude the impact of those on the final results.

In order to provide insight on the model choice and the sensitivity of results to model improvement we have selected for each process of relevance to high-temperature air flows a conventional, simplistic model most widely used in particle simulations, and a more recent model that provides additional fidelity, as proven by validation studies, over the conventional model.

B. Vibration-translation energy transfer

Two different energy models are used in this work to compute the vibration-translation (V-T) energy transfer in collisions of air species. The first one is the conventional LB model, with the vibrational energy levels of an anharmonic oscillator, and temperature-dependent vibrational relaxation numbers $Z_v(T)$. For molecule-molecule collisions, $Z_v(T)$ is determined using the semiempirical Millikan-White correlation [37] with Park's high-temperature correction [38]. For molecule-atom collisions, two sets of recent QCT results are incorporated. Originally developed for O_2-O [39] and N_2-N [13] collisions, the expressions [40] and [13] are adapted here to collisions of O and N atoms, respectively, with all molecular species. For collisions of a molecule with an oxygen

atom [40],

$$Z_v(T) = \begin{cases} 52.46 + 0.04911T - 3.128 \times 10^{-5}T^2, & \text{if} \quad T \leqslant 1000, \\ \exp[5.228 - 0.1405\log(T)], & \text{otherwise.} \end{cases}$$

For collisions of a molecule with a nitrogen atom,

$$Z_v(T) = \tau_v/\tau_c,$$

where [15]

$$\tau_v = \frac{101\,325}{kT}\{\exp[246.747(T^{-1/3} - 0.1193)] + \exp[46.9888(T^{-1/3} - 0.41714)]\},$$

and τ_c is the VHS collision time [27],

$$\tau_c = \frac{1}{2\sqrt{\pi}d^2\sqrt{2kT/m_R}(T_{\text{ref}}/T)^{\omega-0.5}},$$

where d, ω, and T_{ref} are the VHS diameter, exponent, and reference temperature, respectively, and m_R is the reduced mass of the colliding particles.

The above expressions are those directly applicable to continuum simulations; in order to use them in DSMC, a continuum-to-kinetic transformation [41] is applied,

$$Z_v^{DSMC} = Z_v\frac{\zeta_t}{\zeta_t + Z}, \tag{1}$$

where $Z = 0.5\zeta_v^2(T)\exp(\theta_v/T)$, ζ_t and θ_v are the numbers of relative translational and vibrational degrees of freedom, respectively, and θ_v is the vibrational characteristic temperature. The algorithm prohibiting double relaxation is used for the internal mode selection [36].

The high-fidelity model used for V-T of molecule-molecule collisions is the 3D state-to-state forced harmonic oscillator free rotation (FHO-FR) model [42], implemented as discussed in Ref. [43]. Precalculated look-up tables are used for V-T transition probabilities, with the expressions [42] applied for the vibrational deexcitation events, and the detailed balance directly imposed for the reverse excitation collisions. Note that the FHO-FR model [42] and its DSMC implementation [43] have been verified through a comparison with the V-T trajectory calculation results [42] for molecule-molecule collisions.

While the FHO-FR model matches well the trajectory results for molecule-molecule collisions, the molecule-atom interactions are more challenging to capture. This is to a large extent due to significant contribution at high temperatures of the atom-exchange reaction channel. Measurements are not able to distinguish (without special isotopic labeling) postcollision distributions of the molecule internal energy that results from vibrational relaxation versus those that result from atom-exchange reactions. Works such as Refs. [15,39] have shown that the vibrational energy distribution resulting from the atom-exchange reaction appears to be almost independent of the initial (reactant) vibrational level, and depends roughly on the total energy of the collision. This physical behavior is almost exactly the situation that is assumed in the phenomenological LB V-T model discussed above. That is why Ref. [40] demonstrates a very close match between vibrational relaxation calculated for O_2 in collisions with O using QCT, which includes both V-T and atom-exchange reactions, and that calculated using just DSMC V-T process with the LB model and appropriate $Z_v(T)$ values. Since the atoms are indistinguishable, rapid V-T relaxation using the LB model mimics closely the true physics taking place for these homonuclear atom-exchange reactions. Because of this, we simplify our models by not explicitly including homonuclear atom-exchange reactions, but instead using the LB model with the appropriate $Z_v(T)$ values given above for the V-T energy transfer in collisions with atoms.

C. Vibration-vibration energy transfer

The process of vibration-vibration (V-V) energy transfer has often been neglected in the DSMC method and in computational fluid dynamics (CFD) in general, for one obvious reason: its impact is smaller than vibration-translation energy transfer. The V-V transfer does not always significantly, or even visibly, affect the easily observable, and relevant for practical applications, thermodynamic flow properties such as gas density and pressure. Its impacts may generally be regarded as indirect. First, it changes the vibrational populations of molecular species, which in turn changes rates of vibrationally favored reactions, such as dissociation, in nonequilibrium conditions. Second, it redistributes vibrational energy between different air species, most notably, O_2 and N_2. Since CFD methods generally do not take into consideration V-V exchange, it has been turned off in our conventional approach.

In our high-fidelity physical approach, V-V exchange is included due to its correlation with the vibrationally favored dissociation described in the following section. We use the only V-V technique suitable for the DSMC method that is available for collisions of unlike species, the near-resonant V-V transfer model [44]. In that model, V-V transitions may occur only in collisions where the resonance defect is smaller than the prescribed value, 2% in this work, and the transition probability is determined from the local gas temperature. The model was validated in Ref. [44] through comparisons with available relaxation rates in nitrogen-oxygen mixtures. While not taking into consideration all details of the V-V process, it nevertheless captures the process rates and is believed to provide the first-order modeling accuracy on par with that of the LB approach for R-T and V-T exchanges.

D. Dissociation and exchange reactions

The total collision energy (TCE) model of chemical reaction [29] applied in the conventional approach is the most widely used chemistry model in the DSMC method. In the traditional TCE model [29], the reaction is possible when the total collision energy of the colliding pair, E_c, exceeds the reaction threshold, E_d, and the reaction probability P has the following energy dependence:

$$P \propto a_{TCE} \frac{(E_c - E_d)^{b_{TCE}}}{E_c^{c_{TCE}}}.$$

Here, the constants a_{TCE}, b_{TCE}, and c_{TCE} are functions of the parameters A and B in the Arrhenius temperature-dependent reaction rate $k_r(T) = AT^B \exp(-E_d/kT)$, usually determined from measurements, the molecular masses of colliders, and the parameters of the interaction model. The TCE model is always tied to the VHS or variable soft sphere (VSS) [45] model, and using a more complicated intermolecular potential may strip the TCE model of its simple analytic form. The total collision energy E_c is the sum of the relative translational energy of colliding molecules and some specified fraction of the rotational and vibrational energies of the colliding pair. In this work, full contribution from the internal energy modes is assumed. Note that the TCE model may be used for dissociation as well as exchange reactions. The constants A, B, and E_d for all dissociation and exchange reactions in a 5-species air are listed in Table II, and generally follow Ref. [46].

Dissociation of molecular nitrogen and oxygen is one of the most important processes in high-temperature air flows. It significantly impacts thermal properties of the gas and heat fluxes to the surface, as it removes the dissociation energy from the translational and internal modes of molecules, and transfers it to the potential energy of created atoms. The key mechanism that influences the dissociation rate in thermal nonequilibrium is vibrational favoring. Vibrational favoring, sometimes called vibration-dissociation coupling, means that the vibrational energy of the dissociating molecule has a larger impact on the reaction probability than the relative translational and rotational modes. In other words, among two pairs of colliding molecules that have the same total collision energy, the pair where the dissociating molecule has higher vibrational energy will have higher reaction probability. The TCE model does not take into consideration vibrational favoring. In this work, for the high-fidelity approach we have chosen the extended Bias

TABLE II. Constants in the Arrhenius rate and parameters of the Bias model for different reactions. A is in molecules/(m^3 s), E_d is in J.

Reaction	A	B	E_d	A_b	λ_b
$N+O_2 \rightarrow N+O+O$	5.993×10^{-12}	-1.0	8.197×10^{-19}	0.12	2.0
$NO+O_2 \rightarrow NO+O+O$	5.993×10^{-12}	-1.0	8.197×10^{-19}	0.12	2.0
$N_2 + O_2 \rightarrow N_2+O+O$	1.198×10^{-11}	-1.0	8.197×10^{-19}	0.66	4.0
$O_2 + O_2 \rightarrow O_2+O+O$	5.393×10^{-11}	-1.0	8.197×10^{-19}	1.0	4.0
$O+O_2 \rightarrow O+O+O$	1.498×10^{-10}	-1.0	8.197×10^{-19}	4.0	2.0
$O+N_2 \rightarrow O+N+N$	3.178×10^{-13}	-0.5	1.561×10^{-18}	1.0	2.0
$O_2 + N_2 \rightarrow O_2+N+N$	3.178×10^{-13}	-0.5	1.561×10^{-18}	0.75	4.0
$NO+N_2 \rightarrow NO+N+N$	3.178×10^{-13}	-0.5	1.561×10^{-18}	0.3	2.0
$N_2 + N_2 \rightarrow N_2+N+N$	7.968×10^{-13}	-0.5	1.561×10^{-18}	0.75	4.0
$N+N_2 \rightarrow N+N+N$	6.900×10^{-8}	-1.5	1.561×10^{-18}	1.5	2.0
$N_2+NO \rightarrow N_2+N+O$	6.590×10^{-10}	-1.5	1.043×10^{-18}	0.06	2.0
$O_2+NO \rightarrow O_2+N+O$	6.590×10^{-10}	-1.5	1.043×10^{-18}	0.06	2.0
$NO+NO \rightarrow NO+N+O$	1.318×10^{-8}	-1.5	1.043×10^{-18}	1.5	4.0
$O+NO \rightarrow O+N+O$	1.318×10^{-8}	-1.5	1.043×10^{-18}	1.0	2.0
$N+NO \rightarrow N+N+O$	1.318×10^{-8}	-1.5	1.043×10^{-18}	1.0	2.0
$O+NO \rightarrow O_2+N$	5.279×10^{-21}	1.0	2.719×10^{-19}		
$O+N_2 \rightarrow NO+N$	4.000×10^{-17}	0.25	5.288×10^{-19}		
$N+O_2 \rightarrow NO+O$	1.598×10^{-18}	0.5	4.968×10^{-20}		
$N+NO \rightarrow N_2+O$	8.890×10^{-18}	0.25	0.0		

model [47,48] which provides a simple way to adjust the degree of vibrational favoring, and thus fit the reaction probability to available theoretical and experimental data.

In the Bias model, the dissociation occurs when $E > E_d$ with a probability

$$P_d = A_b\left(1 - \frac{E_d - E_v}{E - E_v}\right)\exp\left[\lambda_b\left(\frac{E_v}{E_d} - 1\right)\right], \tag{2}$$

where E is the sum of the relative translational energy of the colliding pair and the internal energy of the dissociating molecule, E_v is the molecule's vibrational energy, A_b is the calibration constant chosen to match the benchmark reaction rate constant, and λ_b is the free parameter controlling the degree of vibrational favoring. The value of A_b is expected to be of order unity based on the physical argument for the large probability of dissociation from the highest vibrational level in any collision. A_b may be expected to vary somewhat from unity in a DSMC implementation, given that the phenomenological VHS total collision cross section is not exactly equal to the true cross section based on an accurate scattering potential. The parameters A_b and λ_b were obtained through detailed comparison with available QCT results, as discussed below. Their values are listed in Table II. It is important to note that the values of A_b differ from those recommended earlier [26] for N_2-N_2 collisions. The difference of a factor of two stems from the particular numerical implementation of the Bias model. In the present work, in a collision of two molecules, both molecules are consecutively checked for reaction through the probability given by Eq. (2), whereas only one molecule, chosen randomly from the two colliders, was checked in Ref. [26].

The reaction probability (2) may generally exceed unity for some energies when $A_b > 1$, thus changing the resultant reaction rate. The majorant frequency scheme used in this work to model the collision process allows for a simple work-around to avoid this problem. The majorant frequency for the corresponding colliding species pair is increased, while the nonreactive collision probability is proportionally decreased. Consider N-N_2 collisions with $A_b = 1.5$ as an example. In the simulation, A_b is set to 1 instead of 1.5, but the number of majorant collisions is increased by a factor of 1.5. The bias dissociation algorithm is unchanged, while the nonreactive collision probability is reduced

TABLE III. Parameters of the equilibrium reaction constant $k_E = A_E T^{B_E} \exp[-E_d/(kT)]$ for different dissociating species. A_E is in m^3, E_d is in J.

Species	A_E	B_E	E_d
N_2	1.319×10^{31}	-0.5	1.561×10^{-18}
O_2	1.084×10^{31}	0.0	8.197×10^{-19}
NO	2.409×10^{30}	0.0	1.043×10^{-18}

by a factor of 1.5 during the relative velocity check. Such a modification allows for maintaining the correct number of reactive and nonreactive collisions at the same time, while increasing the total computational time by only several percent. Note also that the intent of this work is to analyze the impact of the model under nonequilibrium conditions. In order to make that comparison more meaningful, we attempted to exclude the impact of the rates where possible, by making the corresponding equilibrium rates used for the TCE and Bias models close.

The TCE model is used in this work for the Zeldovich exchange reactions, with the LB redistribution of energy over the reaction products. Although detailed cross sections from recent QCT studies are available for most Zeldovich reactions (see, for example, the results of Refs. [20,49] and references therein), and Arrhenius-form reaction constants have lately been published [50] that were fitted to QCT data, the exchange reaction rates were found to have little or no impact on the results presented here, and thus their analysis is out of scope.

E. Recombination reaction

Similarly to the V-V process, the collisional recombination reactions were often neglected in DSMC simulations. The main reason is the strong dependence of recombination rates on the gas density n. Since the recombination is the result of three-body interactions, its rates are proportional to n^3, and not n^2, as are dissociation and exchange reaction rates. The DSMC method has traditionally been used for rarefied flows, where gas density is relatively low, and thus the influence of recombination may reasonably be assumed to be limited. However, the recent application of DSMC to higher density, near-continuum flows makes recombination necessary, especially for accurate modeling of surface heat fluxes. To study the impact of three-body recombination, it is included in this work in the high-fidelity approach, but turned off in the conventional approach.

The recombination model used in this work is an empirical microscopic model developed for the DSMC method in Ref. [26]. Compatible with the bias dissociation model, it uses energy-dependent recombination probabilities derived from the temperature-dependent rates presented in the Arrhenius form, and the collision theory for chemical reactions. Importantly, it satisfies the detailed balance requirement for equilibrium gas in order to assign postcollisional internal energies of newly created molecules. The recombination rates are obtained from the corresponding dissociation rates (see Table I) and the equilibrium reaction constants. The latter follow the recommendations of Ref. [51] and are given in Table III.

F. High temperature flow models

In order to examine the impact of the model of key high-temperature processes mentioned in the previous sections, a succession of models listed in Table IV is considered. Here, the notation MB is used for the baseline approach where all models are included that improve simulation fidelity. The approach may therefore be considered high fidelity. MR is the baseline approach, but with recombination reactions turned off. MRC denotes the approach with no recombination reactions, and the TCE model for dissociation instead of the Bias model. In MRCVV, the vibration-vibration transfer is also turned off. Finally, V-T transfer is modeled with LB instead of FHO-FR in MRCVVT. MRCVVT essentially represents the conventional DSMC approach to modeling high-temperature

TABLE IV. Models used in the computations.

Approach \ Process	Recombination	Dissociation	V-V	V-T
MB	Yes	Bias	Yes	FHO-FR
MR	No	Bias	Yes	FHO-FR
MRC	No	TCE	Yes	FHO-FR
MRCVV	No	TCE	No	FHO-FR
MRCVVT	No	TCE	No	LB

air flows. Such a succession allows one to individually analyze each model and process without conducting an excessively large number of simulations.

III. VALIDATION OF THE CHEMICAL REACTION MODEL

From the modeling perspective, the most important process in air flows at temperatures where gas ionization is weak is believed to be dissociation. There are several reasons for this, both physical and numerical. The large heat release due to dissociation significantly impacts thermal properties in the gas phase and at the surface. The transformation of molecules into atoms changes the specific heat ratio of the gas. The particular model of dissociation impacts the recombination reaction modeling, as the two reactions are related through the microscopic reversibility condition. Because of all this, special attention is paid here to the accuracy of the dissociation model. Note here also that some other aspects of the high-fidelity approach, such as V-V and V-T energy transfer, have been examined and partially validated elsewhere [43,44].

Generally, the validation of a chemical model in the DSMC method is challenging due to the kinetic nature of DSMC, which ideally requires information on chemical cross sections for transitions from the specific energy states of reactants to the energy states of reaction products. There are few molecules where such an analysis is possible based on comparison with measurements, and air species are not among them. Experimental data are typically available only for temperature-dependent reaction rate constants, and even those often have significant error bars. Therefore, the primary route for model validation, as well as setting the parameters of the reaction model, becomes comparison with results of trajectory calculations. An example of such a comparison is presented in Ref. [52] where the Bias model was examined and compared to QCT nonequilibrium rates and probabilities for nitrogen dissociation reactions. This study confirmed that physically reasonable values of A_b near unity match the QCT values well. It also concluded that $\lambda_b = 4$ for the molecule collider (N_2-N_2 case) and $=2$ for the atom collider (N_2-N case) matched state-specific QCT well. It was hypothesized that the firm physics basis of the Bias model functional form and the likely similarity of general behavior across diatomic species for dissociation reactions should make the λ_b value of 4 for molecular colliders and λ_b value of 2 for atomic colliders a reasonable estimate to use in O_2 and NO dissociation reactions as well. Comparisons with QCT shown below for O_2 dissociation, as well as in an earlier work for the O_2-O case [53], provide strong support for this hypothesis.

Such a validation is conducted below for the Bias model, and its parameter A_b was chosen to give a reasonable match with the best equilibrium reaction rate constant (generally the one obtained by QCT) at a temperature of interest. Comparison for $O_2 + O_2$ with results of Ref. [19] shows that $A_b = 1$ provides good agreement for a temperature of 8000 K. That value was therefore used here as the most representative. The temperature-dependent equilibrium reaction rate constant of the Bias model is plotted in Fig. 1 (left) along with the QCT result [19] and the recommendation [54] based on available experimental data. Hereafter, the DSMC equilibrium reaction rate constant was computed in a heat bath where the number of reactions was counted but the reactions where not modeled, so that the Maxwellian distribution of molecular velocities and the Boltzmann distribution

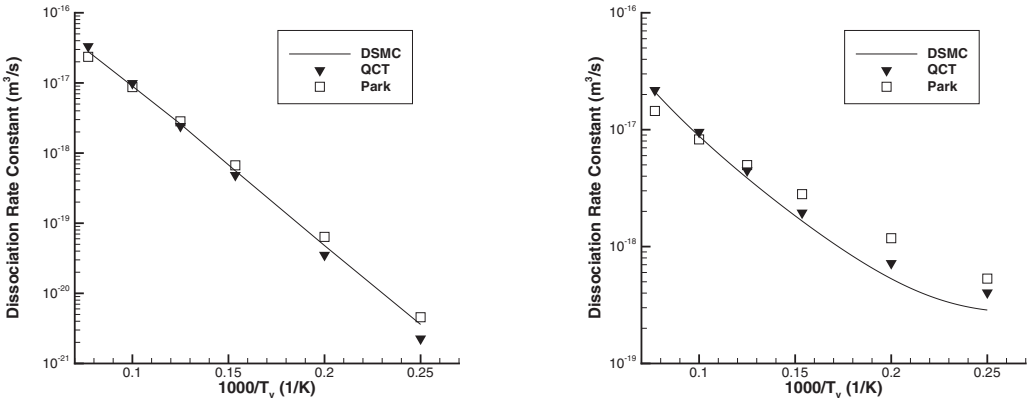

FIG. 1. $O_2 + O_2$ equilibrium (left) and nonequilibrium (right) dissociation rate computed with different approaches. The nonequilibrium case is shown for translation and rotation temperature of 10 000 K.

of internal energies are maintained. The slope of the reaction rate constant curve is not impacted by A_b, and only weakly depends on λ_b. Nonetheless, the form of the reaction probability (2) results in a nearly exponential dependence of the reaction rate constant on temperature T for $T \ll E_d/k$, and thus there is good agreement between all three rates. For higher temperatures, the Bias model agrees better with QCT, and for lower temperatures, with Park's expression [54].

While the parameter A_b determines the equilibrium reaction rates, λ_b to a large extent determines the rates in nonequilibrium conditions, when the vibrational temperature differs significantly from the rotational and translational ones. Larger values of λ_b result in a higher degree of vibrational favoring, when the reaction probability is more sensitive to the vibrational level of the dissociating molecule, and the dissociation rate therefore strongly depends on the vibrational temperature. As with $N_2 + N_2$, a value of $\lambda_b = 4$ provides reasonable agreement with QCT data, with the difference of not worse than 50% for temperatures up to 15 000 K. This is illustrated in Fig. 1 (right), where the rate constant is shown at a fixed $T_{\text{trn}} = T_{\text{rot}} = 10\,000$ K and varying T_{vib}. It also has a somewhat stronger vibrational favoring than the two-temperature Park model [54]. The DSMC nonequilibrium rate constant was computed in a Maxwell-Boltzmann gas where the reactions were counted but not modeled, and the vibration-translation energy transfer was forbidden. While the equilibrium rate matching is necessary for model comparison and applicability analysis, it is also important to compare the energy-dependent reaction probabilities, since they are directly used in DSMC computations. Such a comparison is given in Fig. 2, where the reaction probability is shown in a 10 000 K thermal bath for different vibrational and rotational energies of the dissociating molecule normalized by the dissociation energy. The DSMC result is obtained using the Bias model applied to all colliding pairs after the VHS velocity check selecting physical collisions was conducted. As seen in Fig. 2 (right), there is a strong dependence of that probability on vibrational energy, where the molecules residing at highest vibrational levels are almost four orders of magnitude more likely to react than lowest-level molecules. There is an excellent agreement between the Bias model and the QCT [19] for the lower half of the vibrational energy spectrum. For the higher levels, the Bias model predicts approximately 30% to 50% higher probabilities. As expected, the dependence on the rotational energy is much weaker (see Fig. 2, left). The Bias model captures the correct trend of increasing the reaction probability with rotational level due to the incorporation into the reaction probability of a dependence on the sum of translational and rotational energies. In the original weak vibrational Bias model [47], there was no such dependence, and thus dissociation probability does not change with rotational level. The Bias model results in an approximately factor of two weaker slope than what was obtained in QCT computations, which may still be considered acceptable. The Bias model does not predict the increase of probability for smallest rotational energies, but that,

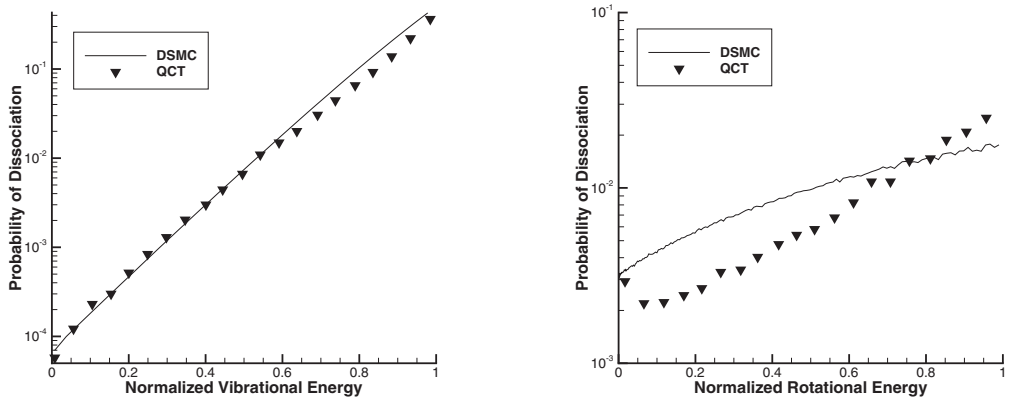

FIG. 2. Dependence of $O_2 + O_2$ dissociation probability on rotational (left) and vibrational (right) energy of dissociating molecule in Bias model and QCT [19].

even if real, should not impact flow results due to low population of the corresponding levels, and their negligible contribution to the dissociation rate.

An important property that may be expected to impact gas properties is the vibrational energy removal due to dissociation, i.e., the amount of energy transferred from the vibrational modes of molecules to the potential energy of reaction products, and thus effectively removed from the flow. Larger energy removal may lead to smaller vibrational temperatures, and thus lower dissociation rates. The average vibrational energy removed from the flow in a single dissociation event at full thermal and chemical equilibrium is plotted in Fig. 3 (left). The DSMC results obtained here using the Bias model are compared to QCT results [19], as well as several continuum CFD models [54,55] also calculated by the authors of Ref. [19]. This is the only case where there is a qualitative disagreement between the Bias model and QCT: the energy removal slightly decreases with gas temperature for the Bias model, and increases for QCT. That makes the Bias model similar to the Sharma model [55] and the conventional one-temperature CFD. The only other model that predicts such an upward trend is the two-temperature Park model. However, the key parameter here is the magnitude of the removal, and not its slope, which is small for all models shown. And the Bias model is relatively close in this respect to QCT, being within 3% for higher temperatures and about 15% for lower temperatures.

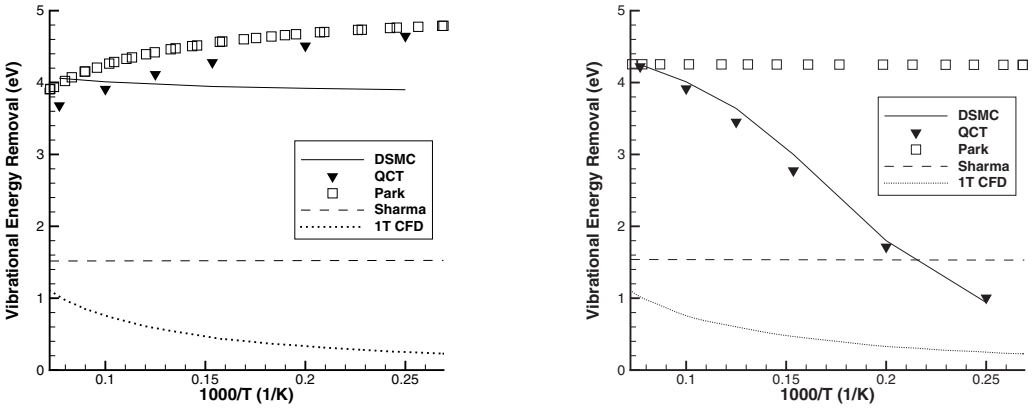

FIG. 3. Vibrational energy removed due to O_2-O_2 dissociation: comparison with QCT [19] and continuum CFD [54] in equilibrium gas with $T_t = T_r = T_v$ (left) and nonequilibrium gas with $T_t = T_r \neq T_v$ (right).

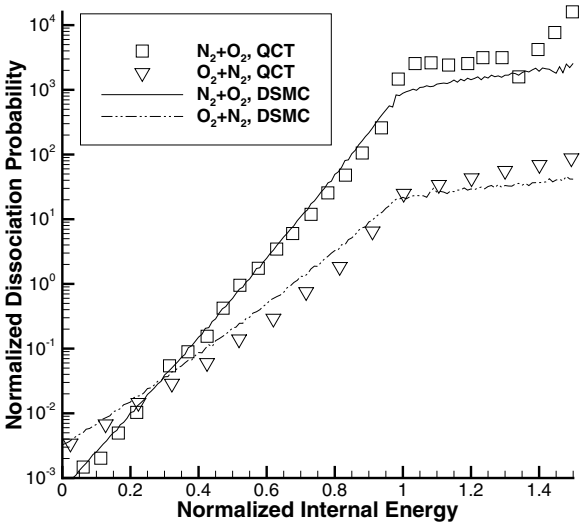

FIG. 4. Energy dependence of oxygen and nitrogen dissociation probabilities obtained in Bias model and QCT calculations [19].

Even more importantly, the Bias model captures the nonequilibrium trend of the vibrational energy removal. This is illustrated in Fig. 3 (right), where the removal is shown at a fixed $T_{\text{trn}} = T_{\text{rot}} = 10\,000$ K and changing vibrational temperature. Both the DSMC and QCT indicate significant decrease in vibrational energy removal with temperature, from over 4 eV per dissociative collision for a vibrational temperature of $T_{\text{vib}} = 13\,000$ K to less than 1 eV for $T_{\text{vib}} = 4000$ K. The difference between the two curves does not exceed 10% for the considered range of temperatures. Such a trend is not predicted by the other three models examined in Ref. [19].

All validation results presented above are for the $O_2 + O_2$ dissociation, which was considered in Ref. [19] in most detail. Other collision species pairs were also tested with the Bias model. All of them were found to agree well with available QCT data after proper selection of the A_b parameter and the already set value of λ_b. An example is shown in Fig. 4 for two other dissociation reactions. In this figure, the dissociation reaction probability normalized by its average value is presented versus the internal energy of the dissociating molecule normalized by the dissociation energy for an equilibrium heat bath at 10 000 K. The Bias model of DSMC is compared to the QCT results [19]. For both computations, the slope changes when the internal energy exceeds unity. This is because for smaller energies, the sharp increase in probability is primarily due to the contribution of vibrational energy. For internal energies larger than E_d, there always has to be some contribution from rotational modes in order to overcome the reaction threshold. The impact of rotations on dissociation is relatively small, as was shown earlier. Similarly to O_2-O_2 dissociation, the dissociation probability in the Bias model is less sensitive to the rotational energy than in QCT; still, the general agreement between the models is good.

IV. SHOCK STANDOFF DISTANCE: SENSITIVITY TO MODEL

There are several basic properties of the hypersonic flow that may be affected by models used for inelastic and reactive processes, which may be grouped into three categories, (i) gas-phase flow properties, such as density and temperature, (ii) surface parameters, both integral and distributed, and (iii) radiation signatures in ultraviolet to infrared spectral regions. The third category is out of the scope of the present work, and is a topic of separate investigation. Here, we consider the model impact on the gas-phase and surface properties for different free stream conditions at flow velocities below 7 km/s, so that the impact of gas ionization may be neglected.

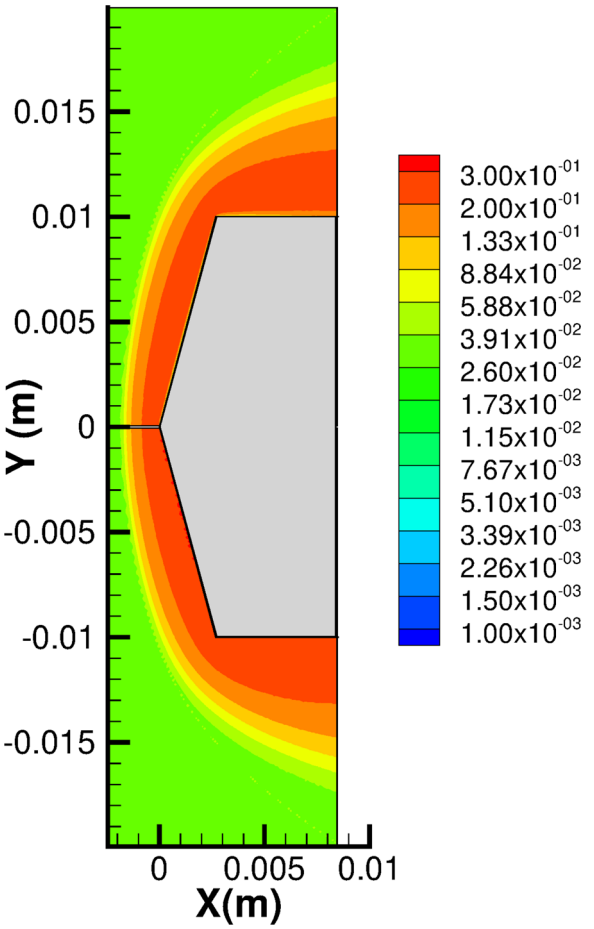

FIG. 5. Atomic nitrogen mole fraction in a dissociating nitrogen flow over a 75 deg cone computed with the high-fidelity (top) and conventional (bottom) models.

As mentioned and discussed in detail in Ref. [8], one of the processes most sensitive to inelastic relaxation effects is the shock detachment process. Measurement of a standoff distance of a shock front from a body in hypersonic flow may present a convenient platform for model analysis and validation, since is provides an opportunity to obtain highly accurate results for a range of flow conditions and geometrical configurations. Moreover, a significant amount of data has been already accumulated for hypervelocity flows of various gases over blunt [56] and sharp geometries [8]. In the latter work, an axially symmetric flow over cones of different angles was examined, and holographic interferograms were recorded in order to obtain standoff distances. In the present work, the conditions of N_2-3 runs (Table 3.2 of Ref. [8]) were reproduced, where the free stream velocity and pressure were 4.97 km/s and 8.91 kPa, and the free stream translation-rotation and vibration temperatures were 1700 K and 3500 K, respectively. Two cone diameters were used, 2 cm and 4 cm, which are expected to be the most sensitive to the real gas effect model, and which manifested some disagreement between measurements and the companion CFD simulations [8]. While different DSMC approaches were used in this work, as listed in Table IV, only the most different ones, MB and MRCVVT, are shown here.

An example of the flow field comparison for these two approaches is given in Fig. 5, where the mole fraction of atomic nitrogen is plotted. In both approaches, there is a significant amount of dissociation observed, as the mole fraction climbs from its free stream value of 0.036 to about 0.3

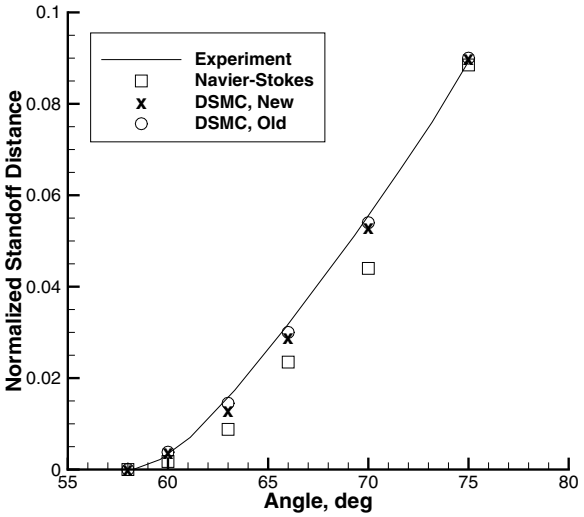

FIG. 6. Shock standoff distance as a function of cone angle in a nitrogen flow: comparison with data [8].

behind the shock. That indicates significant impact of dissociation process. However, there is no visible influence of the model: neither of the high-fidelity effects included in the MB approach have played a role. The general flow structure appears identical for MB and MRCVVT, with the only notable exception of the thin layer near the wall: the gas-phase recombination reduces the number of atoms in that region (this effect will be discussed in more detail in the following sections).

The dependence of the computed and measured shock standoff distance, normalized by the cone diameter, on the cone angle is presented in Fig. 6 for a 2 cm diameter cone. Two DSMC approaches are shown here (the results for the other models fall between these two limits), and also compared to a CFD computation [8] obtained using a Navier-Stokes solver [57]. The key conclusion which may be drawn from that figure is that even though the degree of dissociation is considerable, there is little impact of the high-temperature flow model on the standoff distance. As may be expected, the vibrationally favored dissociation results in a somewhat slower relaxation, and thus shorter standoff distance. However, this difference amounts to only a few percent. Both DSMC results are close to the measurement, and are generally within the numerical and experimental error bars. Clearly, while the good agreement validates the general approach, it does not allow for model differentiation. Also, there is some difference between the DSMC and Navier-Stokes computations, the reasons for which are not quite clear but may partially be attributed to differences in reaction rates. The results for a 4 cm diameter cone, not shown here, indicate an excellent agreement between all simulations and the measurements. Note that a detailed CFD analysis of the standoff distance in reactive air flow over a hemisphere has been conducted in Ref. [58] for significantly higher free stream density. In that work, the impact of the model was found to be on the order of 5%, and all models also underpredicted measurements by approximately that amount. Generally, using the standoff distance as a validation tool for a high-fidelity approach may be fairly challenging due to high resolution necessary to distinguish small differences in models.

V. SHOCK WAVES IN DISSOCIATING OXYGEN

While the shock wave standoff distance has shown little sensitivity to the change in the real gas effect model, detailed flow properties inside the shock wave may give better insight into the model accuracy and applicability. Experimental data [2,59] provide vibrational temperature profiles of O_2 in an oxygen shock under highly nonequilibrium conditions. The temperatures were obtained by measurements of absorption coefficients at different UV wavelengths, and comparing the ratios of

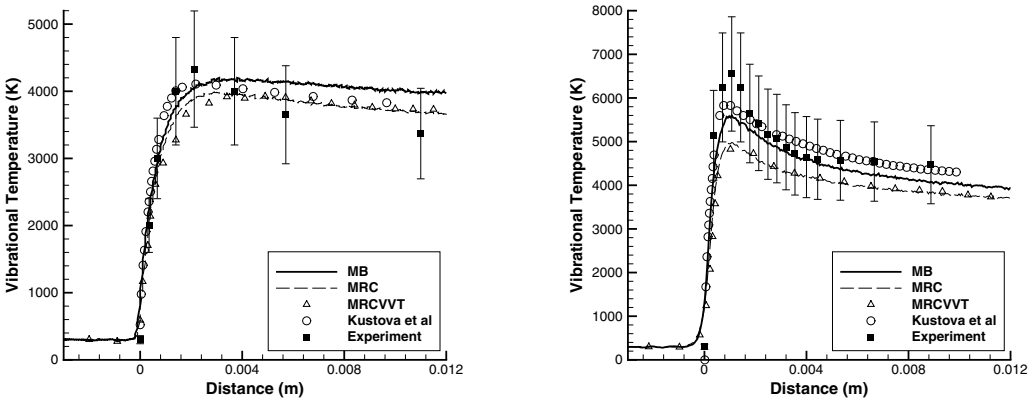

FIG. 7. Vibrational temperature in shock wave of dissociating oxygen: comparison with data [2] for 3.07 km/s (left) and 4.44 km/s (right).

those with calculated theoretical values. Experimental data [2] have been used for model validation in the past [20,60,61] but have been proven to be challenging to match even after significant variation of model parameters [60].

Comparison of different DSMC approaches with the experimental data [2] for two flow velocities is presented in Fig. 7. In this plot, three DSMC approaches are given as well as the solution of one-dimensional equations with the FHO model of V-T energy transfer and a generalized Treanor-Marrone model of dissociation [61]. For both flow cases, the TCE model results in lower vibrational temperature as compared to the Bias model. This is attributed to the influence of the vibrational-dissociation coupling in the Bias model, which decreases the number of dissociation reactions in the Bias model through the depletion of population of upper vibrational levels. Behind the shock wave, it results in the formation of a slowly changing quasisteady state with underpopulated upper levels similar to the flow observed in Ref. [13]. There is very little impact of the vibrational model, V-V as well as V-T, in both cases. Note that recombination reactions also do not impact the temperature in the considered length scale, with the results for MR and MB approaches identical and thus not shown here.

The solution obtained for the MB approach and that of Ref. [61] differ somewhat. The difference is within approximately 5% to 7% for both flow velocities. and may be considered reasonable taking into consideration distinct chemical and vibrational relaxation rates and models used to describe the relaxation process. The disagreement between the DSMC and the experiment is larger, especially in the aftershock region for the lower velocity, and near the maximum temperature at the high velocity. Even though the high-fidelity DSMC approach MB provides a better agreement with the data, the maximum difference still reaches almost 20%. Note though that according to the authors of Ref. [2], the experimental error bars near the temperature peak as well as downstream of it may be as high as 20% due to measurement and temperature deduction uncertainties. Such 20% error bars are indicated in Fig. 7. Remarkably, practically all numerical predictions, even with a conventional DSMC approach, fall within these error bars. Clearly, significant reduction of error bars, preferably to about 5%, would be required to provide the basis for DSMC model evaluation. Even better accuracy may be needed in order to distinguish between a high-fidelity DSMC and a non-DSMC approach. That task however may prove to be extremely difficult and not necessarily worthwhile due to a number of challenges associated with error bar reduction for highly nonequilibrium hypersonic flows.

VI. SURFACE PROPERTIES ON A DOUBLE CONE

As shown above, analysis of flow properties and model validation in hypersonic flow represents an extremely challenging task due to a surprisingly low sensitivity of basic flow properties to the

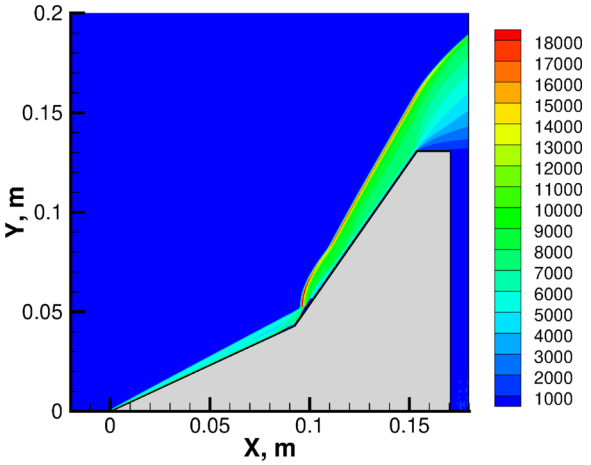

FIG. 8. Translational temperature field over a double cone for LENS run 4 reacting flow conditions.

choice in the high-temperature nonequilibrium flow model, and thus the need for strong reduction in experimental error bars. Surface parameters such a pressure and especially heat flux may provide an additional or an alternative tool for model evaluation. Recent experimental study of aerothermodynamics of a double-cone model in high-enthalpy flow of air [9] have a potential to offer such a tool due to several reasons. The data were obtained in a fairly new LENS XX shock tunnel. The large size of the tunnel ideally should provide free stream conditions that are well defined and free of free stream uncertainties that plagued earlier similar experiments [3]. The data were obtained for widely varied flow enthalpies, with flows from weakly reacting to highly reacting. Experiments were conducted in air, and thus all real gas effect processes should be engaged.

Comparison with experimental data [9] is presented below, conducted for two different flow conditions, both for a double-cone geometry with two conical sections, a 92.1-mm, 25-deg front section and a 61.6-mm, 55-deg rear section. The first condition, which corresponds to run 4 of Ref. [9], has a free stream velocity of 6497 m/s, density of 0.964 kg/m^3, and temperature 652 K; the total stagnation enthalpy is 21.77 MJ/kg and $M = 12.82$. The second condition is that of run 1, which has an enthalpy of 5.44 MJ/kg and $M = 12.2$, with a free stream velocity of 3,246 m/s, density of 0.499 kg/m^3, and temperature 175 K. In order to illustrate the general structure of the flow, the gas translational temperature field is shown in Fig. 8 for run 4 conditions. It can be seen that the temperature behind the oblique shock in front of the first cone is between 4000 K and 5000 K, which indicates that while the vibrational mode should be fully excited, the impact of chemical reactions may be expected to be limited in that region. Note also that the oblique shock interacts with the boundary layer immediately behind the corner point, which results in pressure and heat flux peaks in that region, as will be shown below. The temperature in front of the rear cone is much higher, approximately 8000 K, falling from its peak of up to 20 000 K inside the shock wave. Significant dissociation of air species should therefore occur in that region.

The pressure and heat flux distributions over the double-cone surface are shown in Fig. 9 for run 4 conditions. In addition to experimental data [9], the results of high-fidelity Navier-Stokes computations [62] which use a Marrone-Treanor coupled vibration-dissociation-vibration (CVDV) model are also plotted here. Comparing the high-fidelity (MB) and the conventional (MRCVVT) DSMC approaches, one can see that there is no visible difference in surface pressure, and the only difference in the heat flux is at its peak, where it amounts to approximately 7%. The parameters near the separation region are nearly identical for the two approaches. All this indicates that the impact of the nonequilibrium model, both thermal and chemical, is small. This conclusion is generally consistent with published results. The authors of Ref. [63] have concluded that for run 4 there is no

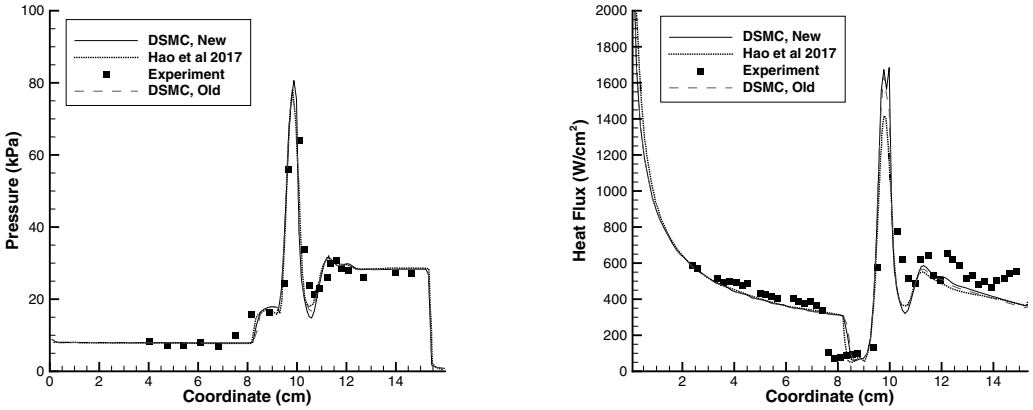

FIG. 9. Comparison of computed and measured [9] surface pressure (left) and heat flux (right) on a double cone for LENS run 4 conditions.

significant difference in prediction of surface heat transfer and pressure between the nonreactive and Park models. The authors of Ref. [62] have used two reaction models, and only a small difference in the separation region was observed. In Ref. [64], a low-enthalpy flow over a double cone was modeled, and although numerical predictions agree well with available experimental data, there is no significant effect of the real gas effect model; it was also noted there that a double wedge may be a better geometry for model validation. Note that all these results were obtained using continuum CFD methods and models.

The present work indicates that the difference in surface properties obtained with a high-fidelity DSMC approach and a CFD method is nearly as small as between CFD methods, and attributed mostly to reaction rates. The difference between the numerical predictions and the measurements is considerably more pronounced. Most notably, the measured separation region is nearly twice as large as those obtained in CFD and DSMC computations. In addition, the measured heat flux is systematically higher on the front and the rear cone sections. The reason for such discrepancies is not clear at this time, but is not likely to result from nonequilibrium high-temperature models. Comparison of simulated and measured surface properties for run 1 conditions of relatively low enthalpy is given in Fig. 10. Here, only the high-fidelity DSMC approach is shown since the results for the conventional approach are nearly identical. The figure shows that the DSMC and CFD profiles are very similar both for pressure and heat flux. There is some small difference in heat fluxes

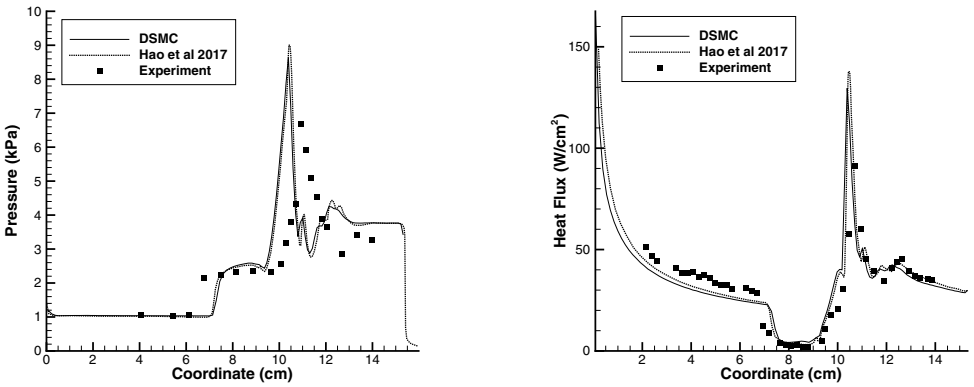

FIG. 10. Comparison of computed and measured [9] surface pressure (left) and heat flux (right) on a double cone for LENS run 1 reacting air flow conditions.

TABLE V. Free stream conditions for HEG comparisons.

Free stream	HEG-I	HEG-III
Velocity (m/s)	5956	4776
Pressure (Pa)	476	687
Temperature (K)	901	694
$X[N_2]$	0.754	0.736
$X[O_2]$	0.007	0.134
X[NO]	0.01	0.051
X[N]	0.0	0.0
X[O]	0.229	0.079

at the first cone, which likely is due to thermal nonequilibrium in the flow, where Navier-Stokes solutions are known to lose accuracy. All other differences are within the numerical error bars related to the parameters of the modeling approach. Similarly to run 4, numerical simulations do not match the experimental results. Here again they underpredict the separation region, although by a smaller amount. On the first cone, the measured heat flux is significantly higher, and that difference cannot be attributed to real-gas effects as their effect is likely smaller. The agreement on the second cone is reasonable for the heat flux, but the pressure profiles are quite different. The reason for the discrepancy is not known to the authors, and one of the possibilities may be that the free stream parameters used in the computations differ somewhat from the experimental conditions.

VII. HIGH-ENTHALPY FLOW OVER A CYLINDER

Inconclusive comparison for the double-cone configuration has prompted us to consider yet another geometry for which hypersonic flow testing has been conducted, a cylinder examined in the HEG shock tunnel [65,66]. The cylinder has a radius of 45 mm, and since its spanwise dimension is much larger, 380 mm, the flow may be modeled as two-dimensional. The advantage of the cylindrical geometry as compared to a double cone [9] is that its blunt shape results in a strong shock wave where the gas temperature reaches normal-shock values, and the impact of real-gas effects and thermal and chemical nonequilibrium may be more pronounced. The disadvantage is that catalytic effects on the surface, shown to be relatively small for a double-cone configuration [9], are significantly more pronounced in HEG experiments. Two free stream conditions were considered here, HEG-I and HEG-III [66], with the flow parameters summarized in Table V.

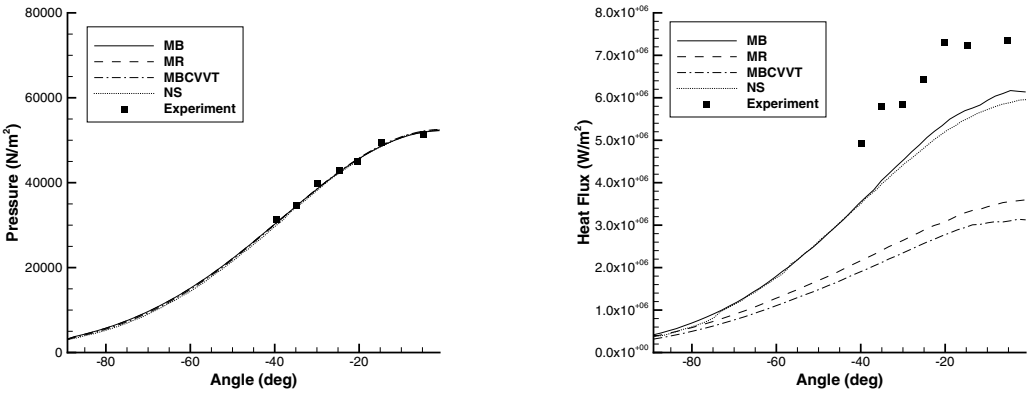

FIG. 11. Impact of model and comparison with data [66] for surface pressure (left) and heat flux (right) in reacting air over a cylinder at HEG-I flow conditions.

The surface properties obtained with three DSMC approaches for HEG-I conditions are compared to the measurements in Fig. 11. The Navier-Stokes computation of Nompelis [66] that did not include catalytic reactions at the surface are also plotted here. As seen in Fig. 11 (right), all numerical results agree with the experiment for the distributed pressure, and there is no discernible difference between various numerical models. That difference is very pronounced for the heat flux, though. Comparison of the high-fidelity DSMC result with the Navier-Stokes solution indicates that the DSMC curve is approximately 5% higher. There are several possible reasons for that difference, and the recombination reaction modeling is only one of them. There could also be some impact of dissociation and exchange reaction rates. The large difference between MB and MR curves shows that the impact of the gas-phase recombination reactions is very significant, as taking into consideration recombination increases the heat flux by over 75%.

This recombination effect is the largest in the heat flux, as all other effects are significantly weaker (compare MR and MRCVVT curves). Nearly all of that MB vs MR difference is attributed to the nitrogen recombination, since the NO recombination is relatively rare, and oxygen recombination is followed by fast dissociation due to significantly lower reaction threshold. Note that both nitrogen recombination rate and recombination model may impact the heat flux distribution, as the first one directly changes the number of recombination reactions and thus the heat released to the flow, while the second changes vibrational populations of N_2 and thus influences the dissociation

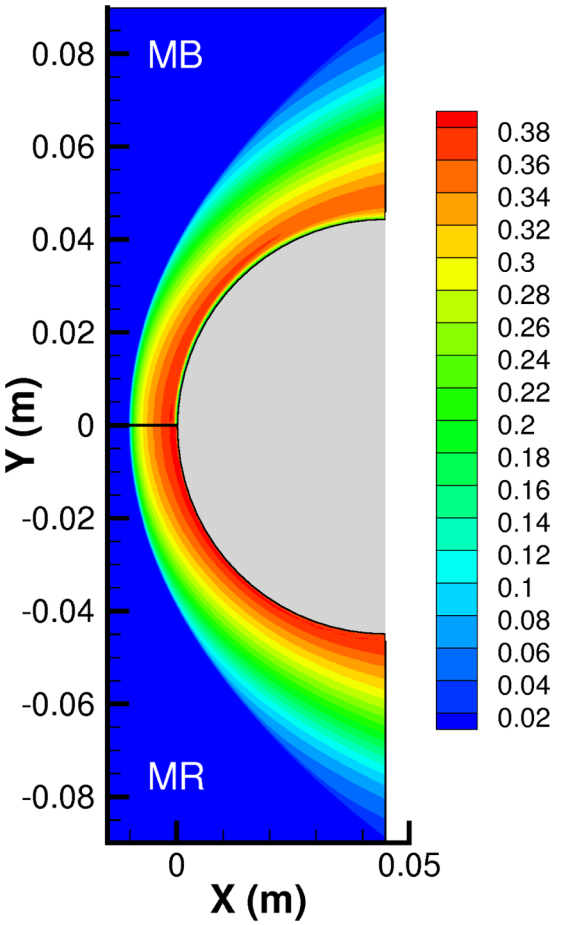

FIG. 12. Atomic nitrogen mole fraction in reacting air flow over a cylinder at HEG-I conditions for the high-fidelity model with (top) and without (bottom) recombination reactions.

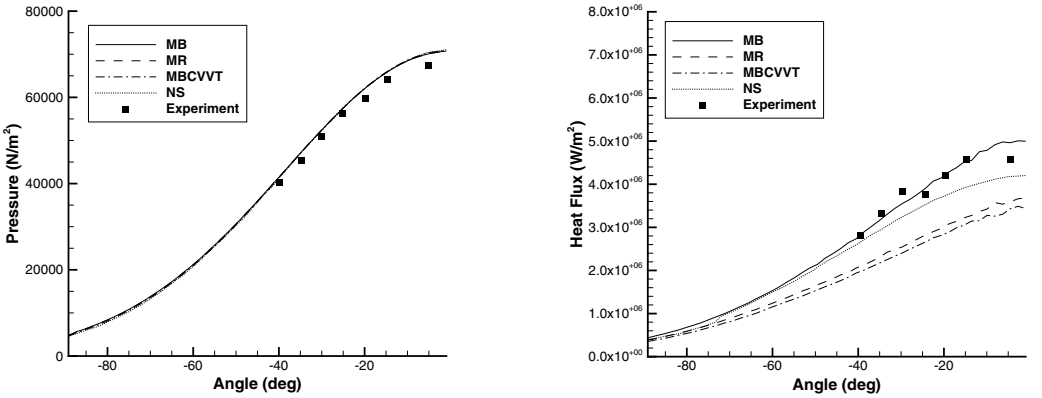

FIG. 13. Computed and measured [66] surface pressure (left) and heat flux (right) on a cylinder at HEG-III air flow conditions.

rate. Vibrational energy accommodation may also play some role. The experimental data points lie noticeably above all numerical curves, including the NS one. The difference between the NS result and the measurement was attributed [66] to the surface catalysis, and including it resulted in matching the data, provided a fully catalytic surface is assumed. The present results indicate that the gas-phase recombination process may be as important as the surface process, and thus may warrant a separate study.

The computations show that the recombination reactions occur almost exclusively in a very thin layer near the cylinder surface. This is illustrated in Fig. 12 where the mole fraction of atomic nitrogen is plotted for the high-fidelity DSMC approach with and without gas recombination reactions. It can be seen that the recombination does not affect the flow beyond a thin surface layer, as the mole fraction (and all other gas properties, not shown here) elsewhere in the flow does not change. In that surface layer, however, the atomic nitrogen mole fraction changes rapidly from almost 0.38 to about 0.08 in the vicinity of the wall. The atomic oxygen mole fraction does not change significantly in that region, staying approximately at 0.2.

The surface properties for the low-enthalpy flow of HEG-III are shown in Fig. 13. Similarly to HEG-I, a noncatalytic result of Nompelis [66] is chosen for the Navier-Stokes curve. Note that the surface catalysis effect was shown [66] to be a significantly smaller factor for this case. Comparison of pressure distributions (Fig. 13, left) indicates that it is not affected by the change in the model or numerical approach, and thus effectively defined only by the free stream conditions. The experimental points fall by a few percent lower than the modeling, which may be related to some uncertainty in the free stream properties. The heat flux differs for all approaches shown, although that difference is generally smaller than for the high-enthalpy case HEG-I. The difference between MB and Navier-Stokes is somewhat larger in the HEG-III case as compared to HEG-I. A dedicated study may be needed to clarify the contribution of various factors in this case, such as the recombination model and rates, the dissociation model, as well as vibrational energy accommodation at the wall, especially for higher v levels. First steps in this direction were made in Refs. [67,68] where near-wall effects and processes in a shock layer have been examined.

VIII. CONCLUSIONS

Validation of high-temperature DSMC models of reacting air has traditionally been challenging due to scarce experimental and theoretical data available in the literature. Recent advances in computational chemistry and high-enthalpy shock tunnel research have a potential to facilitate the task of kinetic model analysis and discerning between different collisional relaxation models. In this work, two DSMC approaches are examined and compared to quasiclassical trajectory results

and experimental measurements: a conventional approach based on the Larsen-Borgnakke method for energy redistribution and the total collision energy for dissociation and exchange reactions, and a high-fidelity approach. The former is based on the state-of-the-art inelastic and chemical reaction rates. The latter one incorporates the FHO-FR model of V-T energy transfer, a general V-V energy transfer model, the vibrationally coupled bias dissociation model, and a consistent recombination process. The primary objective of the work is to analyze the impact of internal energy transfer and reaction model on high-temperature gas flows with significant thermal and chemical nonequilibrium.

The present work has two notable constraints: (i) it only considers neutral flows, which caps flow velocities at approximately 7 km/s so that the air ionization may be neglected, and (ii) only gas and surface properties are examined, and not radiation signatures. The main reason for the constraints is that both of them may well be topics of separate and quite extensive studies. Several conclusions can be drawn from the results of this work. First, a simple Bias model provides sufficient accuracy to quantitatively capture the main features of dissociation of air species. Second, for the flow conditions and models considered in this work, the impact of refinement of internal energy transfer and chemical reaction model is relatively minor for both flow fields and surface properties. V-V and V-T models were found to provide little impact on surface properties. Available experimental data may not offer the means necessary to distinguish between the models, and reducing experimental error bars down to 5% or below may be necessary in order to accomplish that task. Gas flow parameters are more sensitive to models, and time-resolved radiation signature data, especially for high velocities, could provide a valuable tool in model analyses. Third, the impact of gas-phase recombination in the vicinity of the wall was shown to be dominant for a flow over a cylinder, and more study of that process, often omitted in DSMC, may be necessary.

ACKNOWLEDGMENTS

The work was supported by the Air Force Office of Scientific Research. Computational support HPCMP (Project AFPRD04682021) is appreciated.

[1] B. A. Cruden and A. M. Brandis, Measurement and prediction of radiative non-equilibrium for air shocks between 7-9 km/s, in *Proceedings of the 47TH AIAA Thermophysics Conference* (AIAA, Reston, VA, 2017), Paper AIAA 2017-4535.

[2] L. B. Ibraguimova, A. L. Sergievskaya, V. Yu. Levashov, O. P. Shatalov, Yu. V. Tunik, and I. E. Zabelinskii, Investigation of oxygen dissociation and vibrational relaxation at temperatures 4000–10800 K, J. Chem. Phys. **139**, 034317 (2013).

[3] M. MacLean, T. P. Wadhams, M. S. Holden, and R. Parker, A computational analysis of thermochemical studies in the LENS facilities, in *Proceedings of the 45TH Aerospace Sciences Meeting and Exhibit* (AIAA, Reston, VA, 2007), Paper AIAA 2007-0121.

[4] A. B. Swantek and J. M. Austin, Heat transfer on a double wedge geometry in hypervelocity air and nitrogen flows, in *Proceedings of the 50th AIAA Aerospace Sciences Meeting including the New Horizons Forum and Aerospace Exposition* (AIAA, Reston, VA, 2012) Paper AIAA 2012-0284.

[5] D. E. Gildfind, R. G. Morgan, M. McGilvray, R. J. Stalker, and T. N. Eichmann, Free-piston driver optimisation for simulation of high Mach number scramjet flow conditions, Shock Waves **21**, 559 (2011).

[6] C.-Y. Wen and H. G. Hornung, Non-equilibrium dissociating flow over spheres, J. Fluid Mech. **299**, 389 (1995).

[7] C. E. Treanor, I. V. Adamovich, M. J. Williams, and J. W. Rich, Kinetics of nitric oxide formation behind shock waves, J. Thermophys. Heat Transfer **10**, 193 (1996).

[8] I. Leyva, Shock detachment process on cones in hypervelocity flows, Ph.D. thesis, Caltech, 1999.
[9] M. S. Holden, M. MacLean, T. P. Wadhams, and A. Dufrene, Measurements of real gas effects on regions of laminar shock wave/boundary layer interaction in hypervelocity flows for blind code validation studies, in *Proceedings of the 21ST AIAA Computational Fluid Dynamics Conference* (AIAA, Reston, VA, 2017), Paper AIAA 2013-2837.
[10] V. Parekh, D. Gildfind, S. Lewis, and C. James, X3 expansion tube driver gas spectroscopy and temperature measurements, Shock Waves **28**, 851 (2018).
[11] M. McGilvray, L. Doherty, R. Morgan, and D. Gildfind, T6: The Oxford University Stalker tunnel, in *Proceedings of the 20th AIAA International Space Planes and Hypersonic Systems and Technologies Conference, Glasgow, Scotland* (AIAA, Reston, VA, 2015), Paper AIAA 2015-3545.
[12] Z. Li, N. Parsons, and D. A. Levin, A study of internal energy relaxation in shocks using molecular dynamics based models, J. Chem. Phys. **143**, 144501 (2015).
[13] P. Valentini, T. E. Schwartzentruber, J. D. Bender, I. Nompelis, and G. V. Candler, Direct molecular simulation of nitrogen dissociation based on an *ab initio* potential energy surface, Phys. Fluids **27**, 086102 (2015).
[14] P. Valentini, T. E. Schwartzentruber, J. D. Bender, and G. V. Candler, Dynamics of nitrogen dissociation from direct molecular simulation, Phys. Rev. Fluids **1**, 043402 (2016).
[15] M. Panesi, R. L. Jaffe, D. W. Schwenke, and T. E. Magin, Rovibrational internal energy transfer and dissociation of $N_2(^1\Sigma_g^+)$-$N(^4S_u)$ system in hypersonic flows, J. Chem. Phys. **138**, 044312 (2013).
[16] A. Guy, A. Bourdon, and M.-Y. Perrin, Derivation of a consistent multi-internal-temperature model for vibrational energy excitation and dissociation of molecular nitrogen in hypersonic flows, in *Proceedings of the 51st AIAA Aerospace Sciences Meeting* (AIAA, Reston, VA, 2013), Paper AIAA 2013-0194.
[17] F. Esposito, I. Armenise, G. Capitta, and M. Capitelli, O-O_2 state-to-state vibrational relaxation and dissociation rates based on quasiclassical calculations, Chem. Phys. **351**, 91 (2008).
[18] D. Andrienko and I. D. Boyd, Master equation study of vibrational and rotational relaxations of oxygen, J. Thermophys. Heat Transfer **30**, 533 (2016).
[19] R. S. Chaudhry, M. S. Grover, J. D. Bender, T. E. Schwartzentruber, and G. V. Candler, Quasiclassical trajectory analysis of oxygen dissociation via O_2, O, and N_2, *Proceedings of the 2018 AIAA Aerospace Sciences Meeting, AIAA SciTech Forum* (AIAA, Reston, VA, 2018), Paper AIAA 2018-0237.
[20] H. Luo, M. Kulakhmetov, and A. Alexeenko, Ab initio state-specific N_2+ O dissociation and exchange modeling for molecular simulations, J. Chem. Phys. **146**, 074303 (2017).
[21] D. Bose and G. V. Candler, Thermal rate constants of the N_2+ O $\rightarrow$ NO + N reaction using *ab initio* $^3A''$ and $^3A'$ potential energy surfaces, J. Chem. Phys. **104**, 2825 (1996).
[22] D. Bose and G. V. Candler, Simulation of hypersonic flows using a detailed nitric oxide formation model, Phys. Fluids **9**, 1171 (1997).
[23] B. Sebastiao, M. Kulakhmetov, and A. Alexeenko, DSMC study of oxygen shockwaves based on high-fidelity vibrational relaxation and dissociation models, Phys. Fluids **29**, 017102 (2017).
[24] B. Sebastiao and A. Alexeenko, Consistent post-reaction vibrational energy redistribution in DSMC simulations using TCE model, Phys. Fluids **28**, 107103 (2016).
[25] C. Zhang and T. E. Schwartzentruber, Inelastic collision selection procedures for direct simulation Monte Carlo calculations of gas mixtures, Phys. Fluids. **25**, 106105 (2013).
[26] S. F. Gimelshein and I. J. Wysong, DSMC modeling of flows with recombination reactions, Phys. Fluids **29**, 067106 (2017).
[27] G. A. Bird, *Molecular Gas Dynamics and the Direct Simulation of Gas Flows* (Clarendon Press, Oxford, 1994).
[28] M. S. Ivanov, G. N. Markelov, and S. F. Gimelshein, Statistical simulation of the transition between regular and Mach reflection in steady flows, Comput. Math. Appl. **35**, 113 (1988).
[29] G. A. Bird, Monte Carlo simulations in an engineering context, in Proceedings of the 12TH nternational Symposium on Rarefied Gas Dynamics, Charlottesville, VA, Prog. Astronaut. Aeronaut. **74**, 239 (1981).
[30] M. Capitelli, C. Gorse, S. Longo, and D. Giordano, Collision integrals of high-temperature air species, J. Thermophys. Heat Transfer **14**, 259 (2000).

[31] C. Borgnakke and P. S. Larsen, Statistical collision model for Monte Carlo simulation of polyatomic gas mixture, J. Comput. Phys. **18**, 405 (1975).
[32] S. F. Gimelshein, I. D. Boyd, and M. S. Ivanov, DSMC modeling of vibration-translation energy transfer in hypersonic rarefied flows, in *Proceedings of the 33rd Thermophysics Conference* (AIAA, Reston, VA, 1999), Paper AIAA 99-3451.
[33] J. G. Parker, Rotational and vibrational relaxation in diatomic gases, Phys. Fluids **2**, 449 (1959).
[34] F. E. Lumpkin III, B. L. Haas, and I. D. Boyd, Resolution of differences between collision number definitions in particle and continuum simulations, Phys. Fluids A **3**, 2282 (1991).
[35] B. L. Haas, D. B. Hash, G. A. Bird, F. E. Lumpkin, and H. A. Hassan, Rates of thermal relaxation in direct simulation Monte Carlo methods, Phys. Fluids A **6**, 2191 (1994).
[36] N. E. Gimelshein, S. F. Gimelshein, D. A. Levin, M. S. Ivanov, and I. J. Wysong, Reconsideration of DSMC models for internal energy transfer and chemical reactions, AIP Conf. Proc. **663**, 349 (2003).
[37] R. C. Millikan and D. R. White, Systematics of vibrational relaxation, J. Chem. Phys. **39**, 3209 (1966).
[38] C. Park, Problems of rate chemistry in the flight regimes of aeroassisted orbital transfer vehicles, in *Proceedings of the 19TH Thermophysics Conference* (AIAA, Reston, VA, 1984), Paper AIAA 1984-1730.
[39] M. Kulakhmetov, M. Gallis, and A. Alexeenko, Ab initio-informed maximum entropy modeling of rovibrational relaxation and state-specific dissociation with application to the O_2+ O system, J. Chem. Phys. **144**, 174302 (2016).
[40] M. Kulakhmetov, I. B. Sebastiao, and A. Alexeenko, Adapting vibrational relaxation models in DSMC and CFD to ab-initio calculations, in *Proceedings of the 46TH AIAA Thermophysics Conference* (AIAA, Reston, VA, 2016), Paper AIAA 2016-3844.
[41] N. E. Gimelshein, S. F. Gimelshein, and D. A. Levin, Vibrational relaxation rates in the direct simulation Monte Carlo method, Phys. Fluids **14**, 4452 (2002).
[42] I. V. Adamovich, Three-dimensional analytic model of vibrational energy transfer in molecule-molecule collisions, AIAA J. **39**, 1916 (2001).
[43] S. F. Gimelshein, I. J. Wysong, and I. V. Adamovich, Direct simulation Monte Carlo application of the three-dimensional forced harmonic oscillator model, J. Thermophys. Heat Transfer **32**, 882 (2018).
[44] S. F. Gimelshein and I. J. Wysong, Modeling of vibration-vibration energy transfer in the DSMC method, J. Thermophys. Heat Transfer **32**, 781 (2018).
[45] K. Koura and H. Matsumoto, Variable soft sphere molecular model for inverse-power-law of Lennard-Jones potential, Phys. Fluids A **3**, 2459 (2001).
[46] J. N. Moss, G. A. Bird, and V. K. Dogra, Nonequilibrium thermal radiation for an aeroassist flight experiment vehicle, in *Proceedings of the 26TH Aerospace Sciences Meeting* (AIAA, Reston, VA, 2016), Paper AIAA 88-0081.
[47] K. Koura, A set of model cross sections for the Monte Carlo simulation of rarefied real gases: Atom-diatom collisions, Phys. Fluids A **6**, 3473 (1994).
[48] D. Wadsworth and I. Wysong, Vibrational favoring effect in DSMC dissociation models, Phys. Fluids A **9**, 3873 (1997).
[49] F. Esposito and I. Armenise, Reactive, inelastic, and dissociation processes in collisions of atomic oxygen with molecular nitrogen, J. Phys. Chem. A **121**, 6211 (2017).
[50] E. V. Kustova, A. S. Savelev, and O. V. Kunova, Rate coefficients of exchange reactions accounting for vibrational excitation of reagents and products, AIP Conf. Proc. **1959**, 060010 (2018).
[51] W. G. Vincenti and C. H. Kruger, *Introduction to Physical Gas Dynamics* (Krieger, Huntington, 1965).
[52] I. J. Wysong and S. F. Gimelshein, Comparison of DSMC reaction models with QCT reaction rates for nitrogen, AIP Conf. Proc. **1786**, 050021 (2016).
[53] S. F. Gimelshein and I. J. Wysong, Modeling hypersonic reacting flows using DSMC with the bias reaction model, in *Proceedings of the 47TH AIAA Thermophysics Conference* (AIAA, Reston, VA, 2017), Paper AIAA 2017-4025.
[54] C. Park, *Nonequilibrium Hypersonic Aerothermodynamics* (John Wiley & Sons, Inc., New York, 1990).
[55] S. P. Sharma, W. M. Huo, and C. Park, Rate parameters for coupled vibration-dissociation in a generalized SSH approximation, J. Thermophys. Heat Transfer **6**, 9 (1992).
[56] C. Wen, Hypervelocity flow over spheres, Ph.D. thesis, Caltech, 1994.

[57] J. Olejniczak, Computational and experimental study of nonequilibrium chemistry in hypersonic flows, Ph.D. thesis, University of Minnesota, 1997.

[58] E. Josyula, C. J. Suchyta, K. Vogiatzis, and P. Vedula, State-to-state kinetic modeling of select air species in hypersonic nonequilibrium flows, in *Proceedings of the 47TH AIAA Thermophysics Conference* (AIAA, Reston, VA, 2017), Paper AIAA 2017-3489.

[59] L. B. Ibraguimova, A. L. Sergievskaya, V. Yu. Levashov, O. P. Shatalov, Yu. V. Tunik, and I. E. Zabelinskii, Equilibrium and non-equilibrium rate constants of oxygen dissociation at high temperatures, AIP Conf. Proc. **1501**, 1094 (2012).

[60] I. Wysong, S. Gimelshein, Y. Bondar, and M. Ivanov, Comparison of DSMC chemistry and vibrational models applied to oxygen shock measurements, Phys. Fluids **26**, 043101 (2014).

[61] E. Kustova, E. Nagnibeda, G. Oblapenko, A. Savelev, and I. Sharafutdinov, Advanced models for vibrational-chemical coupling in multi-temperature flows, Chem. Phys. **464**, 1 (2016).

[62] J. Hao, J. Wang, and C. Lee, Numerical simulation of high-enthalpy double-cone flows, AIAA J. **55**, 2471 (2017).

[63] N. Kianvashrad and D. Knight, The effect of thermochemistry on prediction of aerothermodynamic loading over a double cone in a laminar hypersonic flow, in *Proceedings of the 2018 AIAA Aerospace Sciences Meeting* (AIAA, Reston, VA, 2018), Paper AIAA 2018-1812.

[64] G. Shoev, G. Oblapenko, O. Kunova, M. Mekhonoshina, and E. Kustova, Validation of vibration-dissociation coupling models in hypersonic non-equilibrium separated flows, Acta Astronaut. **144**, 147 (2018).

[65] S. Karl, J. Martinez-Schramm, and K. Hannemann, High enthalpy cylinder flow in HEG: A basis for CFD validation, in *Proceedings of the 33RD AIAA Fluid Dynamics Conference and Exhibit* (AIAA, Reston, VA, 2003), Paper AIAA 2003-4252.

[66] D. Knight, J. Longo, D. Drikakis, D. Gaitonde, A. Lani, I. Nompelis, B. Reinmann, and L. Walpot, Assessment of CFD capability for prediction of hypersonic shock interactions, Prog. Aerospace Sciences **48-49**, 8 (2012).

[67] S. F. Gimelshein and I. J. Wysong, Validation of high-temperature air reaction and relaxation models using emission data, J. Thermophys. Heat Transfer, doi:10.2514/1.T5555 (2019).

[68] S. F. Gimelshein and I. J. Wysong, Gas-phase recombination effect on surface heating in nonequilibrium hypersonic flows, J. Thermophys. Heat Transfer, doi:10.2514/1.T5556 (2018).